Using Real-Time Fusion Imaging Constructed from Contrast-Enhanced Ultrasonography and Magnetic Resonance Imaging for High-Grade Glioma in Neurosurgery

Dong-fang Wu[1], Wen He[1], Song Lin[2], Bo Han[2], Chi-Shing Zee[3]

■ OBJECTIVE: **To compare the observation of high-grade glioma (HGG) based on intraoperative multiplane ultrasonography (US) images and preoperative reconstructive coplanar T1-weighted enhanced magnetic resonance imaging (MRI) using volume navigation (V Nav) fusion image technology.**

■ METHODS: **We retrospectively evaluated intraoperative data obtained from 16 patients diagnosed with HGG (grade III and IV). Overall, 18 nodules observed in 15 patients were examined. HGG images from US and contrast-enhanced US (CEUS) were compared with those from preoperative reconstructive coplanar enhanced T1-weighted MRI using automatic V Nav fusion image technology.**

■ RESULTS: **All HGG tumors were detected. Images of 13 of 18 tumors (72.2%) with obscure margins using B-mode US were improved with clear tumor boundaries using CEUS imaging. The relative difference in tumor area between CEUS and enhanced MRI modalities in 14 mainly solid component lesions was considered statistically significant (*P* value < 0.05). There was a perfect correlation of the enhanced area between coplanar CEUS and enhanced MRI.**

■ CONCLUSIONS: **The V Nav fusion image system combining intraoperative real-time US imaging with reconstructive preoperative coplanar MRI is valuable for image-guided HGG resection. It is suitable for neurosurgeons who lack the expertise in US technology to discern the brain structure and allows better recognition of tumor and edema tissues compared with reconstructive preoperative coplanar-enhanced MRI in real time and in multiplane from different angles. In addition, CEUS combined with B-mode US could improve tumor detection and resection control in neurosurgery, even in single US-guided operations.**

INTRODUCTION

Since the early 1990s, several studies have shown the ability of T1-weighted gadolinium contrast magnetic resonance imaging (MRI) to improve brain tumor detection, diagnosis, and monitoring to enable the resection of brain tumors.[1,2] Many studies have confirmed that contrast-enhancing tumor size is an important prognostic factor that improves overall survival for patients with glioblastoma multiforme, including untreated tumor size, removal of residual tumor area, and extent of surgical resection.[3-5] Thus, although preoperative MRI data are affected by gravity, removal of the brain, and brain tissue deformations during craniotomy, preoperative MRI has been the gold standard for the diagnosis and therapy of malignant gliomas for neurosurgeons in clinical trials for decades.[6-8] However, preoperative MRI is limited to providing detailed images of the tumor and brain anatomy during operation and intraoperative MRI-guided neurosurgery navigation is limited by its complex application, such as requiring a specific portable MRI scanner, and time cost. Up to now, conventional ultrasound (US)-guided neurosurgery has been widely

Key words
- Contrast-enhanced ultrasonography
- Enhanced T1-weighted MRI
- Fusion imaging
- High-grade glioma
- Volume navigation

Abbreviations and Acronyms
CEMR: Contrast-enhanced magnetic resonance
CEUS: Contrast-enhanced ultrasonography
EA: Enhanced area
HGG: High-grade glioma
MRI: Magnetic resonance imaging
TEAS: Tumor enhancement areas subtracted
US: Ultrasonography
V Nav: Volume navigation

From the Departments of [1]Ultrasound and [2]Neurosurgery, Beijing Tiantan Hospital, Capital Medical University, Dong Cheng District, Beijing, China; and [3]Department of Radiology, Keck School of Medicine, University of Southern California, Los Angeles, California, USA

To whom correspondence should be addressed: Wen He, M.D. [E-mail: hewen168@sohu.com]

Citation: World Neurosurg. (2019) 125:e98-e109.
https://doi.org/10.1016/j.wneu.2018.12.215

*Journal homepage: **www.journals.elsevier.com/world-neurosurgery***

*Available online: **www.sciencedirect.com***

used because of the shifting of the brain parenchyma, low cost, its real-time capabilities, repeatability, and lack of radiation exposure.[9,10] However, limitations include its weakness in differentiating between tumor and edema brain tissue.[11,12] One of the main disadvantages in using conventional US for neurosurgery is operator variability, because a US examination depends on the operator's skills and experience. In addition, there is a lack of evidence to prove that intraoperative US is a perfect match to MRI for discerning brain tumors in neurosurgery. Thus, it is vital to combine preoperative MRI with intraoperative US images for the guidance of neurosurgery. For these reasons, a few studies have reported about the fusion imaging technology for an intraoperative real-time US imaging examination combined with preoperative MRI in areas with brain tumors. These studies paid more attention to provide useful information about the tumor location, features, and margins that were acquired to show that intraoperative US images were similar to preoperative MRI with the fusion imaging technology.[13,14] A real-time, fast, and accurate intraoperative image-guided delineation of high-grade glioma (HGG) especially for edema-surrounded tumors is still a challenge. To better accomplish the overall resection of HGG effectively guided by a single intraoperative US imaging modality in the future, the aim of this study is to observe HGG from different angles through intraoperative multiplanar US images and preoperative reconstructive coplanar T1-weighted enhanced MRI using real-time intraoperative fusion imaging (US-MRI) with volume navigation (V Nav) technology during neurosurgery.

METHODS

We retrospectively evaluated intraoperative data obtained from 16 patients diagnosed with HGG (grade III and IV) with preoperative MRI who were willing to undergo fusion imaging examination. A total of 18 nodules in 15 patients with HGG (grade III and IV) according to the World Health Organization 2007 classification included in this study underwent fusion imaging using intraoperative real-time US and contrast-enhanced US (CEUS) with preoperative T1-weighted contrast-enhanced MRI (CEMR) from the Department of Neurosurgery at Beijing Tiantan Hospital (Beijing, China) from December 2016 to February 2018. One patient was excluded because of the detection of lymphoma after neurosurgery. The inclusion criteria included 1) patients with suspected HGG by preoperative MRI scans; 2) patients who were not undergoing treatment, including radiotherapy and chemotherapy; and 3) patients who were older than 18 years. Patients with pacemakers were excluded because of the magnetic interferences of the V Nav system.

Imaging Examination

Before HGG removal, every patient underwent intraoperative US examination using a LogiqE9 equipped with automatic image fusion technology (Volume Navigation [GE Healthcare, Waukesha, Wisconsin, USA]). The 4-point OmniTRAX Active Patient Tracker was fixed onto the head of the patients who were willing to undergo the preoperative MRI scan; during the initial registration of the operation, the 4-point OmniTRAX Active Patient Tracker was fixed in the same position for both US images and MRIs fusion. The C2-7VN-D small convex US transducer (2–7 MHz) was used with an inner position sensor masked with a sterile transducer cover (3L Medical Products Group Co. Ltd., Jiangxi, China). The sterilized covered probe was placed on the dura after the cranial bone was removed but before opening the dura with US gel for acoustic coupling. The V Nav technology with fusion imaging was used to allow fusion of US images with MRI automatically in real time. Anatomic MRI information regarding the size and spatial location of the tumor was provided intraoperatively by shifting the US probe. CEUS examination was accomplished after scanning fusion of B-mode US with MRI; this workflow is shown in Figure 1. Sulfur hexafluoride microbubbles, with 2.5 μm diameter (SonoVue, Bracco, Milan, Italy), were selected as the US contrast agent. The US contrast agent was prepared by mixing 5 mL of 0.9% saline with 59 mg of SonoVue. An aspiration of 2.4 mL was injected into the peripheral vein as a bolus injection and flushed with 10 mL of 0.9% saline. The participants were scanned in a Discovery MR750 3.0-T magnetic resonance system (GE Healthcare, Little Chalfont, United Kingdom) before undergoing neurosurgery 1–3 days later. Contrast-enhanced steady-state T1-weighted images were acquired after the patients received an injection of the contrast agent (gadopentetate dimeglumine, 0.2 mL/kg based on body weight).

Comparison Between Preoperative MRI and Intraoperative US Imaging

Before removal of tumor after opening the cranial bone, the patients underwent fusion imaging examination with intraoperative real-time US and preoperative T1-weighted gadolinium-enhanced MRI. The overlap function was used to testify to the accuracy of the brain anatomy in real time for both the US imaging and MRI modalities. Next, the tumor was scanned by moving the US probe. We analyzed the real-time images from both the B-mode US and CEUS coplanar MRI modalities in terms of tumor location and margins (defined or obscured). In addition, CEUS examinations were carried out focused on regions of interest. The intraoperative US enhancement pattern was analyzed and compared with the preoperative reconstruction from the gadolinium-enhanced T1-weighted MRI. Image analysis was performed by 2 radiologists (D.W. and W.H.) who had more than 10 years of experience in imaging. The 2 radiologists, who were blinded to the study, designed the US and MRI assessments for the focus lesions. The primary outcomes were strongly enhancement areas in the enhanced US images and MRIs. The EAs of all tumors were measured during the peak enhancement phase (3–6 seconds) to strongly differentiate the surrounding brain parenchyma and the tumor. For each tumor, manually drawn EAs were applied on post–sulfur hexafluoride microbubble enhancement images and coplanar reconstruction post–gadolinium enhancement scans in HGG using V Nav technology. The tumor enhancement areas subtracted (TEAS) in T1-weighted gadolinium-enhanced MRI and enhanced US imaging were measured.

We classified the tumors according to their features in the CEUS and CEMR images into the following 5 categories: A, peripheral thin wall smooth ringlike enhancement with no inner enhancement; B, peripheral thick wall nodular ringlike enhancement with no inner enhancement; C, peripheral thick wall nodular ringlike enhancement with inner dotted and short line enhancement; D, uniform hyperenhancement; and E, no enhancement.

Statistical Analysis

The SPSS version 19.0 statistical software (IBM Corp., Armonk, New York, USA) was used to analyze the results. EAs with CEUS

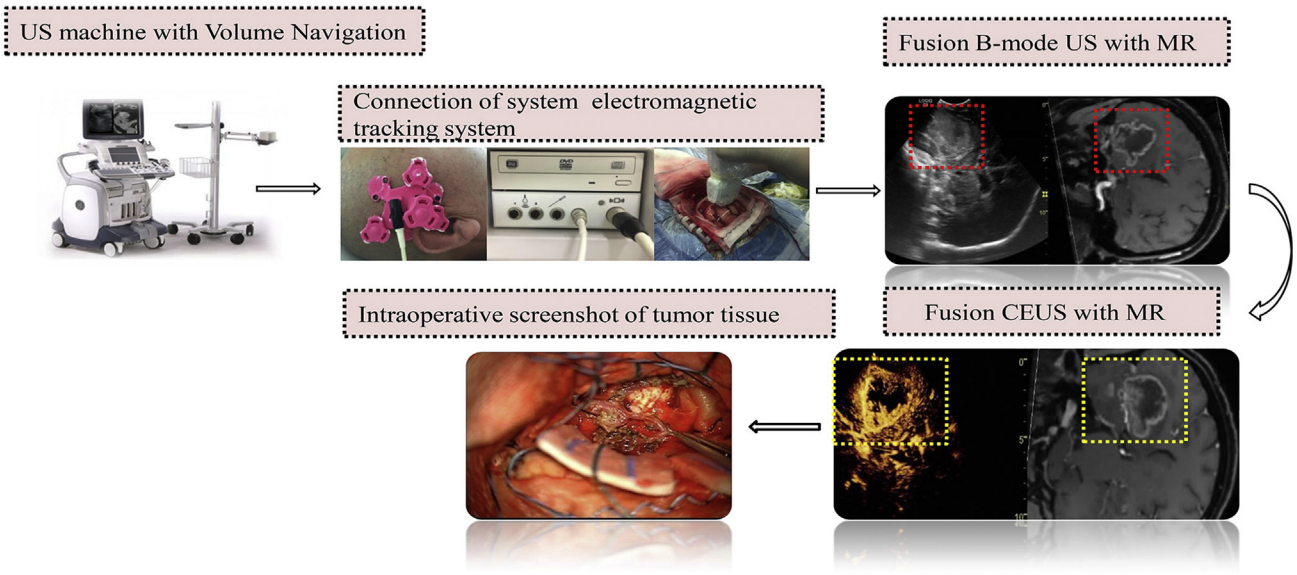

Figure 1. Workflow of Volume Navigation technology (fusion B-mode and contrast-enhanced ultrasonography [US] with preoperative reconstructed enhanced T1-weighted magnetic resonance [MR] imaging)-guided high-grade glioma resection. (*Top row*) US machine equipped with Volume Navigation image fusion technology (*left*). The 4-point OmniTRAXTM Active Patient Tracker was fixed onto the head of the patient. The electromagnetic signal transmitter and the 4-point OmniTRAX Active Tracker were connected to the US machine via local area network. A small convex US probe with an inner position sensor masked with a sterile transducer cover was used (*middle*). Automatic registration of B-mode US image and preoperative magnetic resonance image was successful (*right*). (*Bottom row*) Satisfactory fusion contrast-enhanced US with preoperative T1-weighted enhanced magnetic resonance image (*right*). Screenshot image shows tumor tissue in neurosurgery (*left*).

and CEMR were then analyzed with a paired t test. A *P* value <0.05 was considered statistically significant in all analyses. Pearson correlation analysis was used to assess the relationship between the EAs with sulfur hexafluoride microbubbles as the contrast agent in US images and gadolinium enhancement in MRI. Pearson correlation analysis was used to assess the relationship between TEAS and EAs with sulfur hexafluoride microbubbles as the contrast agent. An overall comparison of sulfur hexafluoride microbubbles and gadolinium enhancement was performed in a random-effects model that considers the correlation between repeated measurements in the same patient. Interobserver agreement was evaluated using the Pearson correlation analysis according to enhanced US images and MRIs with fusion image technology. The closer the Pearson correlation value is to 1.0, the greater the agreement (r value, 0.00–0.20, minimum agreement; 0.21–0.40, intermediate; 0.41–0.60, moderate; 0.61–0.80, substantial; 0.81–1.00, almost perfect).In the statistical analysis, a paired t test was used to determine the intra rater and interrater reliability. A paired t test was calculated using the formula:

$$t = \frac{\overline{X}_1 - \overline{X}_2}{\sqrt{\frac{(n_1-1)S_1^2+(n_2-1)S_2^2}{n_1+n_2-2}\left(\frac{1}{n_1}+\frac{1}{n_2}\right)}}$$

RESULTS

We investigated the use of a V Nav image fusion system combining intraoperative real-time US imaging with preoperative MRIs for image-guided HGG resection in 18 nodules of 15 patients. At the beginning, B-mode US images were shown with fused MRIs on the US machine screen side by side after the automatic registration was successfully processed. The preoperative T1-weighted reconstructed MRIs were changed with respect to the motion of the US probe. All HGG tumors were detected using this US-MRI fusion. After this procedure, fusion imaging obtained from frozen intraoperative US images and preoperative reconstruction coplanar MRIs were overlaid together to evaluate the accuracy of the automatic registration with reference to some anatomic structures such as ventricles. Fifteen patients acquired satisfactory fusion of intraoperative B-mode US with preoperative reconstructive coplanar MRIs. However, 3 tumors of the 18 nodules with B-mode US and MRI fusion failed to match perfectly because these were detected to be mainly cystic component tumors in both modalities. It was not certain if the remaining 15 nodules were deformed because of unclear tumor boundaries. Additional CEUS was performed to observe the tumor margins in all patients. The basic characteristics of the patients with information to differentiate the margins of the HGG tumors with US and CEUS are given in **Table 1**. After observing the B-mode US and enhancement US images, 13 of 18 HGG tumors (72.2%) with obscure margins using B-mode US were improved with clear tumor boundaries using CEUS imaging.

Post–sulfur hexafluoride microbubble enhancement images and coplanar reconstruction post–gadolinium enhancement images were compared for similarities and/or differences from each other.

Table 1. Patients' Basic Characteristics and Margins of Tumors

Patient Number	Age (years)	Sex	Location of Tumor	Grade of Disease	Margins of Tumor in B-Mode Ultrasonography	Margins of Tumor in Contrast-Enhanced Ultrasonography
1	30	M	Right occipitotemporal	III	D	D
2	36	F	Right frontal	II– III	D	D
3	38	M	Right frontal and corpus callosum	IV	O	D
4	64	F	Left occipitotemporal	III	D	D
5	69	F	Right frontoparietal	III	O	D
6	47	M	Left occipitotemporal	IV	O	D
7	59	M	Right temporal insular; left occipital	IV	O/O	D/D
8	62	M	Left occipital	IV	O	D
9	57	M	Right occipital; right frontal	IV	O/O	D/D
10	58	F	Left frontal	IV	O	D
11	52	M	Left occipitotemporal basal ganglia	IV	O	D
12	66	F	Left frontal	IV	D	D
13	35	F	Left frontotemporal; left parietal	IV	O/O	D/D
14	64	F	Left frontal insular	IV	O	D
15	45	M	Right frontal	IV	D	D

M, male; F, female; D, definition; O, obscure.

Then, the CEUS images were shown with synthesized coplanar preoperative enhanced MRIs side by side on the US screen. The enhanced features and EAs of the HGG tumors with 2 coplanar enhancement modality fusion images (CEUS and CEMR) are compared in Table 2. Both radiologists concluded that tumor margins could be traced more easily with CEUS imaging than with B-mode fusion imaging. The 2 radiologists manually traced the EAs of the tumors in CEUS and coplanar CEMR based on the V Nav technology system for 18 nodules. One of the grade II–III gliomas was excluded after comparing the enhancement US image with enhanced MRI to trace the EA of the tumor; the mass showed nearly no enhancement with MRI (Figure 2). The other 3 mainly cystic component tumors with peripheral ringlike thin wall enhancement (classification A) failed to match successfully because of the overall shape of the tumor deformation with B-mode and CEUS images with corresponding coplanar enhanced MRI (Figure 3). Comparing the enhanced thickness of the peripheral ringlike thin wall of the tumor at the largest diameters in the coplanar plane with enhanced MRI and CEUS showed the same enhanced tumor size for the 3 mainly cystic component tumors (0.1–0.38 cm). Thus, for the comparison of the EAs of the tumor between the 2 modalities, 14 nodules that fell into the HGG classification of B, C, and D and for which a successful fusion of the enhancement US images and MRIs was obtained with no obvious deformation to the overall shape of the tumor were included.

The overall comparison of the EA relationship between sulfur hexafluoride microbubbles and gadolinium in a total of 14 nodules is noted later. The relative difference in EA between both enhancement modalities was considered statistically significant ($P < 0.05$). The interobserver agreement with CEUS and CEMR was significant (Pearson correlation = 1.000;, $P < 0.001$) for CEUS-MRI fusion imaging. When the Cronbach $\alpha = 0.05$, the null hypothesis H_o was not rejected. There was no statistically significant difference in intraobserver EA measurements with CEUS and CEMR separately ($P < 0.05$). There was no statistically significant difference in interobserver EA measurements between CEUS and CEMR ($P < 0.05$). The interobserver agreement between radiologist 1 and radiologist 2 was significant (Cronbach $\alpha = 0.99$) for EA measurements with CEUS and CEMR. The results are shown below (Figure 4A and B, Table 3). There was perfect correlation of EA between coplanar CEUS image and enhanced MRI between the 2 radiologists, who manually traced the EAs in the same tumors using 2 different modalities (Figure 5). There was correlation between TEAS and EA size of the tumors in CEUS (Pearson correlation in radiologist 1, $r = 0.812$, $P = 0.000$; Pearson correlation in radiologist 2, $r = 0.711$, $P = 0.004$; Figure 6A and B). Compared with reconstructive coplanar-enhanced MRI in 14 HGG tumors, the tumors showed hyperenhancement, showing that the dense contrast agent microbubbles accumulated more in the tumor than in the peritumoral edema area in enhanced US images. The surrounding edema brain tissue showed that the

Table 2. Post–Sulfur Hexafluoride Microbubble Enhancement Images and Coplanar Reconstruction Post–Gadolinium Enhancement Were Compared

	Types of Tumor Feature		Enhanced Area of Tumor (cm^2) R_1/R_2	
Patient Number	Contrast-Enhanced Ultrasonography	Contrast-Enhanced Magnetic Resonance	Contrast-Enhanced Ultrasonography	Contrast-Enhanced Magnetic Resonance
1	A	A	25.01/25.31	23.22/23.91
2	D	E	16.2/16.9	—
3	C	C	25.82/26.20	22.82/23.10
4	C	C	16.25/16.36	15.17/15.08
5	C	C	21.21/20.90	19.87/19.91
6	C	C	26.35/26.53	23.82/23.85
7	C/C	C/C	7.28/7.30 8.44/8.54	6.51/6.52 7.33/7.30
8	B	B	4.87/4.85	3.54/3.54
9	C/C	C/C	6.97/6.96 16.5/15.9	6.01/6.10 15.8/16.1
10	C	C	23.71/23.75	21.36/21.39
11	B	B	24.73/24.81	22.61/22.69
12	A	A	22.97/22.95	20.65/20.64
13	B/B	B/B	18.50/18.57 6.28/6.30	17.04/17.11 5.84/5.90
14	C	C	20.88/21.02	18.96/19.21
15	A	A	21.87/21.79	20.90/21.06

contrast agent microbubbles perfused nearly in an isoenhanced pattern (Figure 7).

DISCUSSION

In our study, to reduce the registration error of fusion imaging (US-MRI) with the V Nav technology guidance system, intraoperative brain shift, and tissue deformation, the acquired data of regions of interest were selected after making the bone flap but before opening the dura. Before removing the tumor after opening the cranial bone, we first need to justify the precision of register between the US images and MRIs to guarantee that the CEUS image showed the morphologic features of HGG similar to those of the preoperative reconstruction acquired from the gadolinium-enhanced T1-weighted MRIs. Fine-tuning the registration was important to obtain the precision of register based on the reconstruction MRI overlay on the frozen US image so that using the rotational button to move on the X, Y, and Z planes would match in the 2 modalities. This strategy ensured that the fusion image allowed accurate observation of the same tumor plane using the 2 different imaging modalities with the V Nav system.

Application of a real-time fusion image from MRI and US is suitable for mainly solid component HGG.

In our study, HGG was divided into 2 types according to whether the tumor underwent deformation when imaged using fusion image technology after the cranial bone was opened: those with obvious tumor deformation, leading to misregistration in B-mode US with the coplanar MRI; and those with uncertain deformation because of unclear tumor boundaries, which made it difficult to differentiate the tumor from the surrounding edema with B-mode US, but with brain anatomies that accurately matched the coplanar MRI using fine-tuning registration. We found that registration of the tumor on US-MRI fusion failed because of morphologic feature changes in 3 of the tumors, which had mainly cystic components with peripheral smooth ringlike thin walls in B-mode US; these smooth ringlike thin walls showed hyperenhancement (classification A) in both modalities. Furthermore, the location of all 3 tumors was close to the surface of the brain. It is likely that masses with mainly cystic components and that are close to the brain surface are easily deformed after the cranial bone is removed. We hypothesized that mainly cystic component tumors, which are fluid-filled spaces with a peripheral ringlike thin wall, are soft and easy to deform with changes in pressure. Thus, the morphology of mainly cystic tumors would transform following the movement of the brain parenchyma toward the operation hole during the procedure, resulting in deformation. These results show that real-time fusion imaging technology constructed from CEUS with preoperative gadolinium-enhanced MRI is not suitable for tumors that have mainly cystic components with thin walls (classification A) and are near to the brain surface. Furthermore, the EA of classification A tumors in US

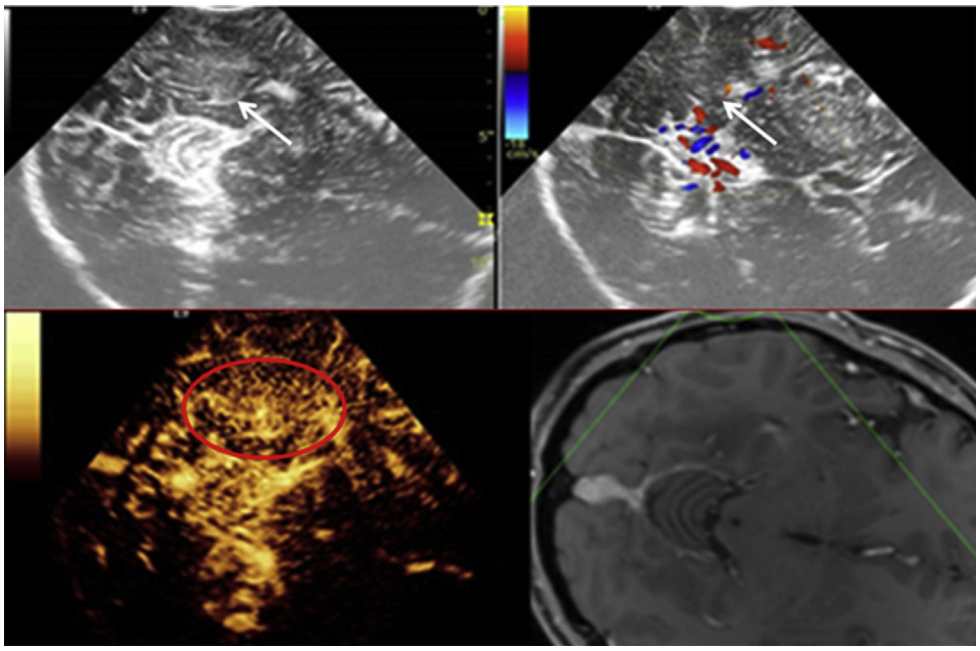

Figure 2. A grade II–III glioma located in the left temporal lobe of a 43-year-old woman. (*Top row*) Screenshot of B-mode ultrasonographic image showing a hyperechoic lesion (*left, arrow*) and color Doppler image showing dotted blood in hyperechoic lesion (*right, arrow*). (*Bottom row*) Fusion contrast-enhanced ultrasound scan shows enhancement of the tumor with clear margins (*left red circle*), while the corresponding coplanar preoperative gadolinium-enhanced T1-weighted magnetic resonance image shows no enhancement of the tumor (*right*).

imaging was almost the same as that in MRI, which showed enhancement in the peripheral ringlike thin wall. HGG tumors with mainly cystic components and that are close to the brain surface would not be ideal for fusion US with MRI because of deformation of the tumor after opening the cranial bone; the single B-mode US image-guidance system as an independent method to guide the operation during neurosurgery is enough for HGG tumors with mainly cystic components surrounded by a ringlike thin wall. In addition, enhanced US-MRI fusion imaging acquired satisfactory morphologic features of 15 of 18 tumors. The shape of mainly solid component tumors was shifted slightly and was corrected using fine-tuning registration before opening the dura. Therefore, the application of a real-time fusion image including T1-weighted enhanced MRI and CEUS would be suitable for mainly solid component HGG.

Fusion CEUS with CEMR could supply neurosurgeons with important information about the EA of the tumor in the same plane but in 2 different modalities during operation.

Up to now, the use of B-mode US remains controversial as a tool for assessing tumor size in malignant gliomas during operation. The greater the extent of surgical resection, the more significant the prolongation of overall survival.[15] Thus, it is important to define the margins of the tumor on the image. With the development of CEUS, it has been widely used for lesions in the liver and other organs to highlight neoplasm neovascularization and analyze the perfusion mode of contrast agents in real time.[16-18] Thus, additional CEUS was performed to observe the tumor margins in neurosurgery; CEUS supplied valuable information such as location, morphology, boundaries, and remnants to neurosurgeons in the area of the brain tumor.[19,20] Most brain tumors were hyperenhanced with CEUS, allowing for better delineation of tumor margins, including identifying necrosis.[21-23] In fusion images with the split-screen modality on a single screen, the CEUS image is shown on the left side and the coplanar synthesized enhanced MRI is shown on the right side.[24] The V Nav system allows for a detailed comparison of intraoperative acquired enhanced US images to coplanar preoperative enhanced synthesized MRI considered as the gold standard of diagnostic modalities in glioma in real time. Thus, the ability to use fusion US images and MRIs to improve the identification of the same brain tumor in 2 modalities including the use of contrast enhancement makes sense for comparing EAs in real time and in coplanar plane images with enhanced US images and MRIs. In our study, after reviewing the B-mode and enhancement US images, 13 of 18 HGG tumors (72.2%) that showed obscure margins with B-mode US had clear tumor boundaries after CEUS imaging was used. CEUS showed better delineation of tumor boundaries than did B-mode US, which made it possible to manually draw EAs on the intraoperative enhanced US images. The comparison of CEUS images with MRIs showed that all the nodules (100%) were hyperenhanced in the CEUS images, whereas 17 of the 18 tumors (94.4%) were enhanced in

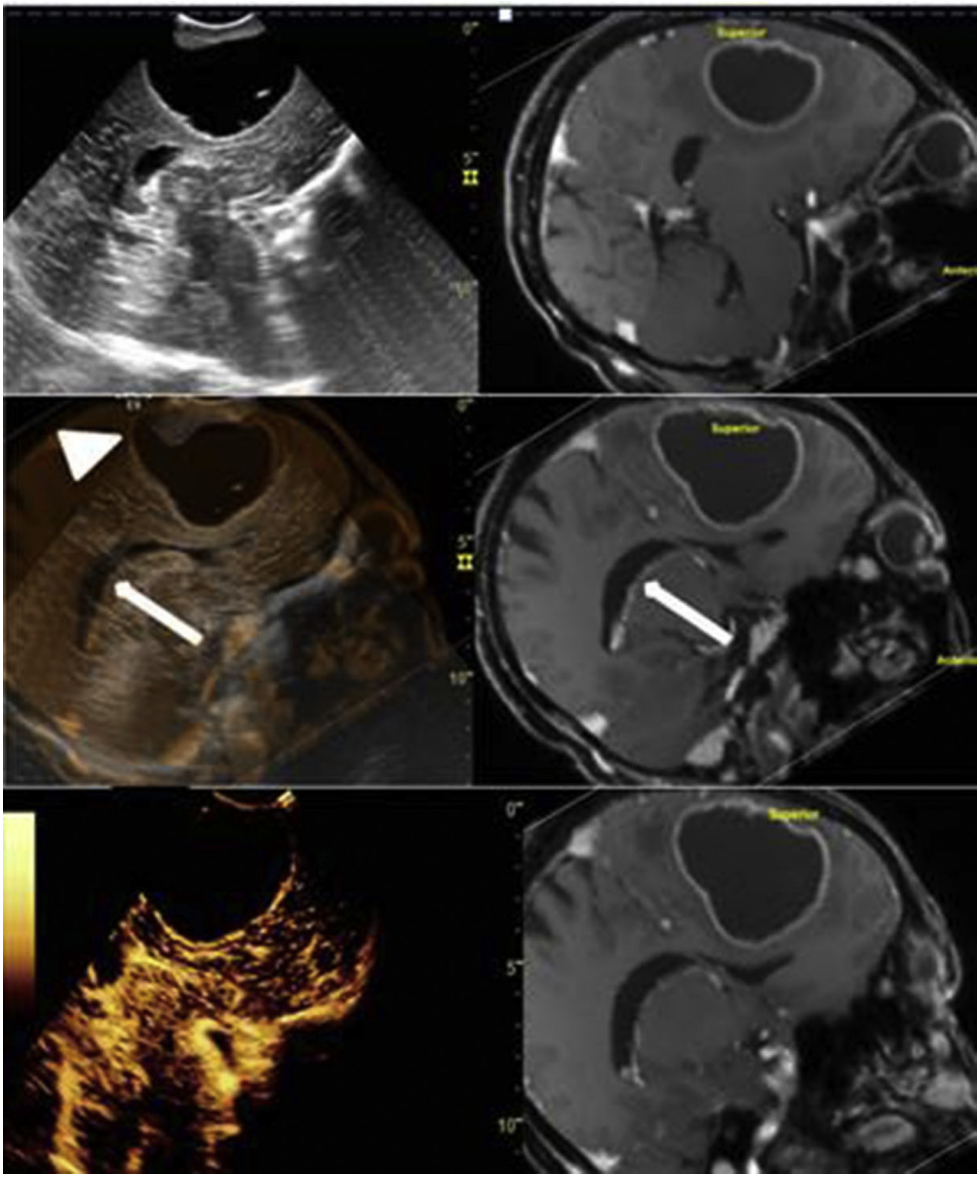

Figure 3. Screenshot of volume navigation (V Nav) system ultrasonopgraphic (US) scans of a left frontal lobe glioblastoma multiforme in a 66-year-old woman. (*Top row*) Fusion image shows a mainly cystic component tumor with thin wall in B-mode US (*left*) and in magnetic resonance imaging (MRI) (*right*). (*Middle row*) The preoperative MRI was overlaid onto the frozen US image side by side after fine-tuning procedures to evaluate the accuracy of the registration in reference to the lateral ventricle structures (*white arrow*) with satisfactory results; the morphology of the cystic component tumor was deformed (*white arrowhead*). (*Bottom row*) Contrast-enhanced US scan showing that the enhancement of the tumor (*left*) was similar to the corresponding coplanar preoperative reconstructed gadolinium-enhanced T1-weighted MRI (*right*).

MRI. The gadolinium contrast did not perfuse the lesion, which was located in the right frontal lobe and was of grade II–III; however, the sulfur hexafluoride microbubble agent filled the tumor with homogeneous less dense contrast agent than in the other tumors in this study. Thus, the case was excluded to manually draw EAs in enhanced MRIs. The same lesion showed different enhanced results in 2 enhancement modality such as CEUS and CEMR because sulfur hexafluoride depends purely on the intravascular distribution of the microbubbles, whereas gadopentetate accumulates within the lesion and also depends on the extent of disruption in the blood-brain barrier.[25] Tumors need enough nutrition to grow, so the formation of new blood

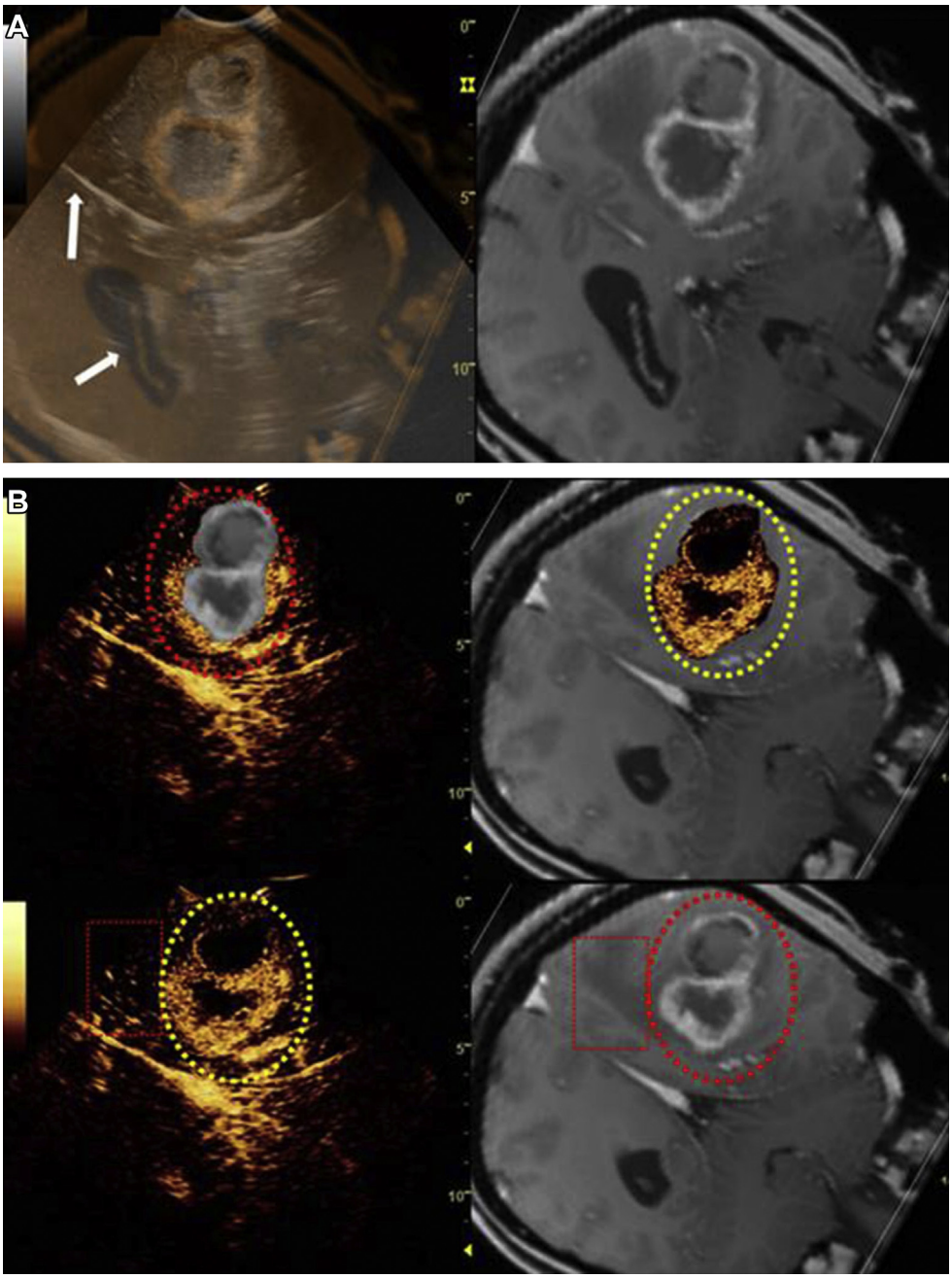

Figure 4. Screenshot of volume navigation (V Nav) system ultrasonographic (US) scans of a left frontotemporal and left parietal lobe glioblastoma multiforme (GBM) in a 35-year-old woman. (**A**) The preoperative reconstructive magnetic resonance image (MRI) was overlaid onto the frozen US image side-by-side to evaluate the accuracy of the registration in reference to the lateral ventricle structures and cerebral falx (*white arrow*) with satisfactory results. (**B**) (*Top row*) The area of the GBM was a little larger in contrast-enhanced US (CEUS) (*red circle*) than in enhanced T1-weighted MRI (*yellow circle*) in overlapping images. (*Bottom row*) Images show the tumor (*yellow circle*) and surrounding edema (*red rectangle*) area enhanced with CEUS and the corresponding coplanar preoperative reconstructed gadolinium-enhanced T1-weighted MRI (*red circle*).

Table 3. Relative Difference in Enhanced Areas Between the Two Contrast Agent Modalities

Radiologist Number	Contrast-Enhanced Ultrasonography ($\overline{X} \pm S$)	Contrast-Enhanced Magnetic Resonance ($\overline{X} \pm S$)	*t* Value	*P* Value	*r* Value
1	16.27 ± 7.98	14.76 ± 7.37	7.395	<0.001	0.998
2	16.28 ± 8.03	14.84 ± 7.42	5.985	<0.001	0.996

vessels is induced.[26] The phenomenon in our study may also be because that tumor, which is a grade II–III glioma, did not show neoangiogenesis, which is observed in higher-grade gliomas.[27]

We measured the EAs of the tumors, including classification B, C, and D tumors, at the largest EA with standardized or unstandardized US planes and reconstruction coplanar magnetic resonance sections. The enhanced tumor area was manually traced in the same plane with 2 different modalities on a split US screen. The 3 mainly cystic component with peripheral ringlike thin wall enhancement (classification A) tumors that failed successful registration between the US image and corresponding coplanar MRI were excluded from the comparison with MRI in the same plane. As a result, the EAs with CEUS in HGG were a little larger than the coplanar reconstructed enhanced MRI during operation. The relative difference in EAs between the US enhancement image and enhanced MRI modalities in 14 lesions with peripheral thick wall nodular ringlike enhancement was considered statistically significant in this study. A possible reason is the difference in enhancement mechanisms of sulfur hexafluoride microbubbles in US and gadopentetate dimeglumine in MRI. The principle for gadolinium enhancement depends on both the tumor vascular phase and degree of disruption of the blood-brain barrier.[25] In addition, gadopentetate dimeglumine enhancement mainly diffuses into the interstitial space from the vasculature; pathologic angiogenesis leads to a tortuous, disorganized, and excessively leaky vasculature with abnormal structure and function in solid tumors. This situation enhances vascular permeability, which in turn is associated with high interstitial fluid pressure.[28-30] Microbubble contrast agents are confined to the intravascular compartment and, hence, sulfur hexafluoride microbubbles enable the visualization of the perfusion of tumor neovascularization.[31,32] This factor could explain the larger EA with CEUS than with coplanar enhanced MRI. Furthermore, a recent study showed that infiltrating glioma cells often exceed the structural imaging boundaries for both low-grade gliomas and HGGs.[33] For HGGs, the difference between the structural and metabolic volumes resulting from volumetric analyses showed that the metabolic volumes were larger than the structural volumes.[34] The other reason why EA with CEUS was a little larger than that with coplanar enhanced MRI may be the deformation by gravity of the brain tumor after opening the cranial bone but before opening the dura. Especially for tumors in which the long axis is vertical to the midline of the brain, when the patient is lying on their side, the sink of the tumor to the midline could cause slight deformation as a result of gravity, resulting in the EA with CEUS being a little larger than that with coplanar enhanced MRI. This is only a guess, and more HGG tumor classification studies are needed. Furthermore, there was perfect correlation of EA between the intraoperative CEUS and corresponding preoperative reconstructive coplanar enhanced MRI in the data, which came from the successful fusion image comparison of US with enhanced MRI, and there was correlation between TEAS and EAs of tumors in CEUS. Thus, we believe that the difference in enhancement mechanisms of sulfur hexafluoride microbubbles and gadopentetate dimeglumine can explain the differences in the EAs. In support of this explanation for the smaller tumor area is the smaller difference in EA between CEUS and enhanced MRI and that the size of the margins of the tumor that needs to be resected is closer to the preoperative MRI tumor area under single US-guidance neurosurgery. Prada et al.[35] compared tumor size on the largest diameters in the axial plane with MRI and CEUS and obtained the same tumor size for 8 of the 10 lesions (80%). We classified the features of the CEUS and CEMR images with HGG into 5 categories, and only classification B, C, and D tumors were included in the study to measure the EA of the tumors after accurate registration of the US images with coplanar MRI using fine-tuning registration. In addition, this was the first time that the EA of HGGs was measured using V Nav technology fusion US images with preoperative reconstructive coplanar MRI not limited to the axial plane in studies observing the size of gliomas. Therefore, the results on tumor EA in our study may be different from those of other reports. The results

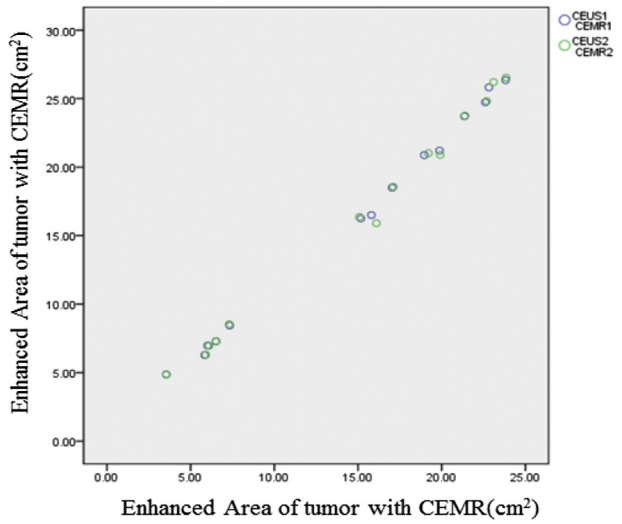

Figure 5. Correlation of enhanced area between contrast-enhanced ultrasonography (CEUS) and contrast-enhanced enhanced area (CEMR) manually traced by 2 radiologists.

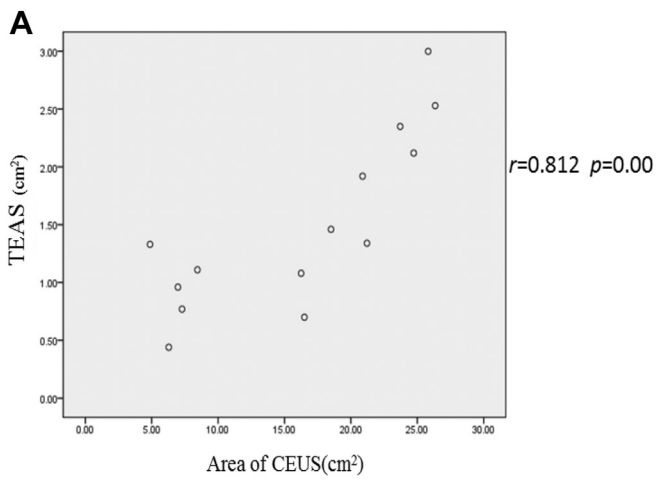

Figure 6. (**A**) Scatterplots showing moderate correlation between the tumor enhancement areas subtracted and enhanced area with contrast-enhanced ultrasonography (CEUS) by radiologist 1. (**B**) Scatterplots showing nearly perfect correlation between the difference in area size and enhanced area with contrast-enhanced ultrasonography by radiologist 2.

showed that the volumes of low-grade gliomas segmented from intraoperative US images were more often smaller than those segmented from preoperative MRIs.[36] However, a large high-quality study focusing on tumor size comparison between US images and MRI remains absent. In our study, we also showed some advantage to intraoperative fusion imaging (US-MR) with V Nav technology; for example, CEUS provided better definition of the tumor borders when peritumoral edema makes them hardly detectable with B-mode US. HGG tumors were hyperenhanced, which showed a denser contrast agent microbubble accumulation pattern than the surrounding edema area in the enhanced US images. This process was vital to differentiate the brain tumor and edema tissue with CEUS, especially compared with coplanar enhanced MRI. The results support that CEUS is needed in US-guided neurosurgery, even in single US. This is an initial study showing the visualization of HGG in 2 different complete coplanar modalities in image-guided neurosurgery. CEUS images can provide neurosurgeons with real-time information for differentiating tumor from normal tissue.[36] Fusion CEUS with CEMR could also supply neurosurgeons with important information about the EA of the tumor in the same plane but in 2 different modalities during operation. We will pay more attention to the differences in tumor EA using fusion imaging with CEUS and CEMR in future studies to accurately delineate the boundary of the tumor and improve gross resection rates under US-guided neurosurgery. Up to now, the application of fusion imaging (US/MRI) has been more suitable for neurosurgeons who lack the expertise in US technology to discern the structure of the brain. The resection of HGG tumors may improve with the use of intraoperative sulfur hexafluoride microbubbles to enhance tumor area with US imaging in the future.

Limitations

There are some limitations that may weaken the results of our study. In this study, we focused only on the comparison of EAs between intraoperative CEUS images and reconstructive preoperative coplanar enhanced MRI using an automatic fusion imaging technology. In future, studies will concentrate on the comparison of EAs between enhanced US images and coplanar enhanced MRI, especially focusing on the different regions between them to acquire biopsy specimens. In addition, the sample size to compare EAs between the 2 coplanar modalities was small in this study and a larger sample is required to better compare the outcomes of fusion imaging in the future. US can provide neurosurgeons with real-time information for differentiating tumor from normal tissue.[36] Fusion CEUS with CEMR could also supply neurosurgeons with important information about the EAs of the tumor in the same plane but through 2 different modalities during operation.

CONCLUSIONS

The use of a V Nav image fusion system combining intraoperative real-time US imaging with reconstructive preoperative coplanar MRI is valuable for image-guided HGG resection. It is not only suitable for application by neurosurgeons who lack the expertise in US technology to discern the structure of the brain but also allows for better recognition of the tumor and edema tissue compared with reconstructive preoperative coplanar enhanced MRI in real time and in multiplane from different angles. In addition, it is proof that CEUS combined with B-mode US could improve tumor detection and resection control in neurosurgery, even in single US-guided operations. However, real-time fusion imaging technology constructed from CEUS with preoperative gadolinium-enhanced MRI is not necessary for all HGG tumors. It is more suitable for mainly solid component brain tumors than mainly cystic component tumors with thin walls and that are near to the brain surface due to the deformation of the tumor after the cranial bone is opened.

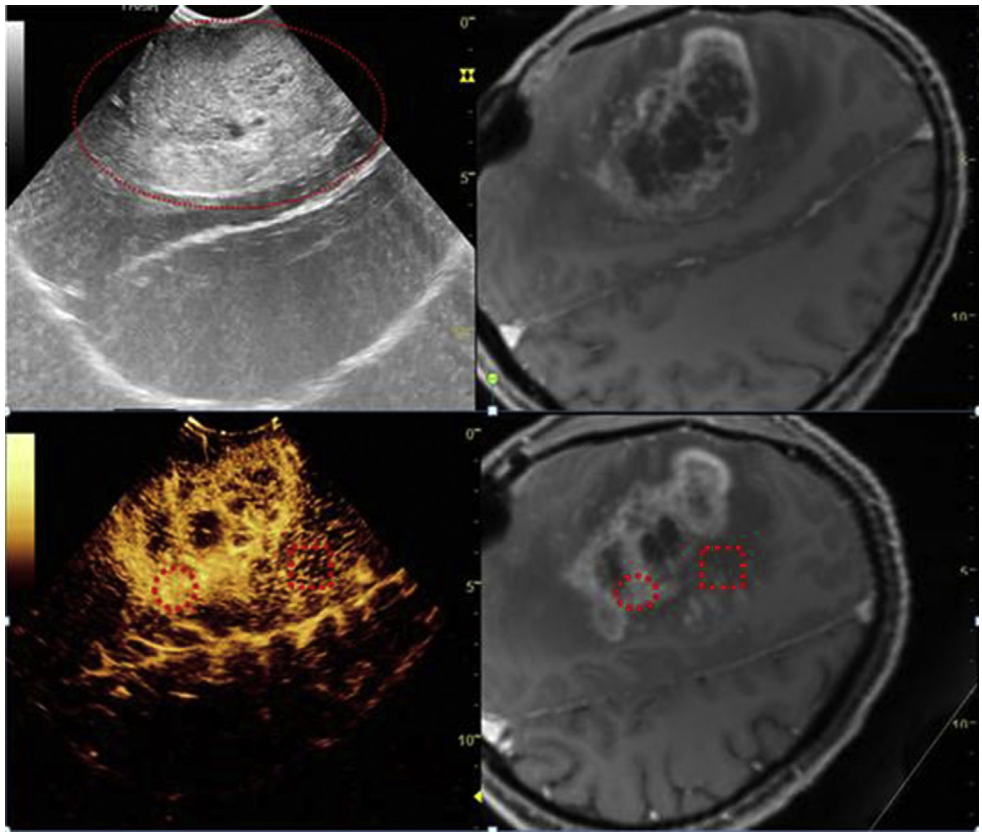

Figure 7. Screenshot of volume navigation system ultrasonographic scans of a left occipitotemporal lobe glioblastoma multiforme in a 47-year-old man. (*Top row*) Fusion image shows a mainly solid component tumor with obscure tumor and edema tissue (*red circle*) in B-mode ultrasound. (*Middle row*) Contrast-enhanced ultrasonography modality (*left*) shows the tumor with hyper enhancement (*red circle*) and peripheral edema (*red rectangle*) was nearly isoenhanced compared with the corresponding coplanar preoperative reconstructed gadolinium-enhanced T1-weighted magnetic resonance imaging (*right*).

REFERENCES

1. Haughton VM, Rimm AA, Czervionke LF, et al. Sensitivity of Gd-DTPA-enhanced MR imaging of benign extraaxial tumors. *Radiology*. 1988;166:829-833.

2. Dean BL, Drayer BP, Bird CR, et al. Gliomas: classification with MR imaging. *Radiology*. 1990; 174:411-415.

3. Aizer AA, Bi WL, Kandola MS, et al. Extent of resection and overall survival for patients with atypical and malignant meningioma. *Cancer*. 2015; 121:4376-4381.

4. Chaichana KL, Jusue-Torres I, Navarro-Ramirez R, et al. Establishing percent resection and residual volume thresholds affecting survival and recurrence for patients with newly diagnosed intracranial glioblastoma. *Neuro Oncol*. 2014;16: 113-122.

5. Pan IW, Ferguson SD, Lam S. Patient and treatment factors associated with survival among adult glioblastoma patients: a USA population-based study from 2000-2010. *J Clin Neurosci*. 2015;22: 1575-1581.

6. Stieglitz LH, Fichtner J, Andres R, et al. The silent loss of neuronavigation accuracy: a systematic retrospective analysis of factors influencing the mismatch of frameless stereotactic systems in cranial neurosurgery. *Neurosurgery*. 2013;72: 796-807.

7. Grabowski MM, Recinos PF, Nowacki AS, et al. Residual tumor volume versus extent of resection: predictors of survival after surgery for glioblastoma. *J Neurosurg*. 2014;121:1115-1123.

8. Rostomily RC, Spence AM, Duong D, McCormick K, Bland M, Berger MS. Multimodality management of recurrent adult malignant gliomas: results of a phase II multiagent chemotherapy study and analysis of cytoreductive surgery. *Neurosurgery*. 1994;35:378-388.

9. Selbekk T, Jakola AS, Solheim O, et al. Ultrasound imaging in neurosurgery: approaches to minimize surgically induced image artefacts for improved resection control. *Acta Neurochir (Wien)*. 2013;155: 973-980.

10. Dohrmann GJ, Rubin JM. History of intraoperative ultrasound in neurosurgery. *Neurosurg Clin North Am*. 2001;12:155-166.

11. Šteňo A, Matejčík V, Šteňo J. Intraoperative ultrasound in low-grade glioma surgery. *Clin Neurol Neurosurg*. 2015;135:96-99.

12. Moiyadi AV. Linear intraoperative ultrasound probes and phased-array probes: two sides of the same coin. *Acta Neurochir (Wien)*. 2015;157:957-958.

13. Prada F, Del Bene M, Mattei L, et al. Fusion imaging for intra-operative ultrasound-based navigation in neurosurgery. *J Ultrasound*. 2014;17: 243-251.

14. Prada F, Del Bene M, Casali C, et al. Intraoperative navigated angiosonography for skull base tumor surgery. *World Neurosurg*. 2015;84:1699-1707.

15. Eyüpoglu IY, Hore N, Merkel A, Buslei R, Buchfelder M, Savaskan N. Supra-complete surgery via dual intraoperative visualization approach (DiVA) prolongs patient survival in glioblastoma. *Oncotarget*. 2016;7:25755-25768.

16. Beyer LP, Wassermann F, Pregler B, et al. Characterization of focal liver lesions using CEUS and MRI with liver-specific contrast media: experience of a single radiologic center. *Ultraschall Med*. 2017;38:619-625.

17. Kazmierski B, Deurdulian C, Tchelepi H, Grant EG. Applications of contrast-enhanced ultrasound in the kidney. *Abdom Radiol (NY)*. 2018;43:880-898.

18. Miyamoto Y, Ito T, Takada E, Omoto K, Hirai T, Moriyasu F. Efficacy of sonazoid (perflubutane) for contrast-enhanced ultrasound in the differentiation of focal breast lesions: phase 3 multicenter clinical trial. *AJR Am J Roentgenol*. 2014;202:W400-407.

19. Arlt F, Chalopin C, Müns A, Meixensberger J, Lindner D. Intraoperative 3D contrast-enhanced ultrasound (CEUS): a prospective study of 50 patients with brain tumours. *Acta Neurochir (Wien)*. 2016;158:685-694.

20. Ritschel K, Pechlivanis I, Winter S. Brain tumor classification on intraoperative contrast-enhanced ultrasound. *Int J Comput Assist Radiol Surg*. 2015;10:531-540.

21. Moiyadi AV. Intraoperative ultrasound technology in neuro-oncology practice—current role and future application. *World Neurosurg*. 2016;93:81-93.

22. Cheng LG, He W, Zhang HX, et al. Intraoperative contrast enhanced ultrasound evaluates the grade of glioma. *Biomed Res Int*. 2016:2643862.

23. Lekht I, Brauner N, Bakhsheshian J, et al. Versatile utilization of real-time intraoperative contrast-enhanced ultrasound in cranial neurosurgery: technical note and retrospective case series. *Neurosurg Focus*. 2016;40:E6.

24. Numata K, Fukuda H, Morimoto M, et al. Use of fusion imaging combining contrast-enhanced ultrasonography with a perflubutane-based contrast agent and contrast-enhanced computed tomography for the evaluation of percutaneous radiofrequency ablation of hypervascular hepatocellular carcinoma. *Eur J Radiol*. 2012;81:2746-2753.

25. Van Dreden P, Elalamy I, Gerotziafas GT. The role of tissue factor in cancer-related hypercoagulability, tumor growth, angiogenesis and metastasis and future therapeutic strategies. *Crit Rev Oncog*. 2017;22:219-248.

26. Nandhu MS, Hu B, Cole SE, Erdreich-Epstein A, Rodriguez-Gil DJ, Viapiano MS. Novel paracrine modulation of Notch-DLL4 signaling by fibulin-3 promotes angiogenesis in high-grade gliomas. *Cancer Res*. 2014;74:5435-5448.

27. Prada F, Mattei L, Del Bene M, et al. Intraoperative cerebral glioma characterization with contrast enhanced ultrasound. *Biomed Res Int*. 2014:484261.

28. Ramjiawan RR, Griffioen AW, Duda DG. Anti-angiogenesis for cancer revisited: is there a role for combinations with immunotherapy? *Angiogenesis*. 2017;20:185-204.

29. Huang Y, Goel S, Duda DG, Fukumura D, Jain RK. Vascular normalization as an emerging strategy to enhance cancer immunotherapy. *Cancer Res*. 2013;73:2943-2948.

30. Bonekamp D, Deike K, Wiestler B, et al. Association of overall survival in patients with newly diagnosed glioblastoma with contrast-enhanced perfusion MRI: comparison of intraindividually matched T1- and T2 (*)-based bolus techniques. *J Magn Reson Imaging*. 2015;42:87-966.

31. Prada F, Bene MD, Fornaro R, et al. Identification of residual tumor with intraoperative contrast-enhanced ultrasound during glioblastoma resection. *Neurosurg Focus*. 2016;40:E7.

32. Artzi M, Blumenthal DT, Bokstein F, et al. Classification of tumor area using combined DCE and DSC MRI in patients with glioblastoma. *J Neurooncol*. 2015;121:349-357.

33. Guo J, Yao C, Chen H, et al. The relationship between Cho/NAA and glioma metabolism: implementation for margin delineation of cerebral gliomas. *Acta Neurochir (Wien)*. 2012;154:1361-1370.

34. Zhang J, Zhuang DX, Yao CJ, et al. Metabolic approach for tumor delineation in glioma surgery: 3D MR spectroscopy image-guided resection. *J Neurosurg*. 2016;124:1585-1593.

35. Prada F, Vitale V, Del Bene M, et al. Contrast-enhanced MR imaging versus contrast-enhanced US: a comparison in glioblastoma surgery by using intraoperative fusion imaging. *Radiology*. 2017;285:242-249.

36. Munkvold BKR, Bø HK, Jakola AS, et al. Tumor volume assessment in low-grade gliomas: a comparison of preoperative magnetic resonance imaging to coregistered intraoperative 3-dimensional ultrasound recordings. *Neurosurgery*. 2018;83:288-296.

Conflict of interest statement: The authors declare that the article content was composed in the absence of any commercial or financial relationships that could be construed as a potential conflict of interest.

Received 27 June 2018; accepted 28 December 2018

Citation: World Neurosurg. (2019) 125:e98-e109.
https://doi.org/10.1016/j.wneu.2018.12.215

Journal homepage: ***www.journals.elsevier.com/world-neurosurgery***

Available online: ***www.sciencedirect.com***